bioRxiv preprint doi: https://doi.org/10.1101/323253; this version posted May 16, 2018. The copyright holder for this preprint (which was not certified by peer review) is the author/funder. All rights reserved. No reuse allowed without permission.

A metal-regulated AMPylation/deAMPylation switch in FIC proteins.

Simon Veyron[1], Giulia Oliva[2,3], Monica Rolando[2,3], Carmen Buchrieser[2,3], Gérald Peyroche[1], Jacqueline Cherfils[1]

[1]Laboratoire de Biologie et Pharmacologie Appliquée, CNRS and Ecole normale supérieure Paris-Saclay, Cachan, France

[2] Institut Pasteur, Biologie des Bactéries Intracellulaires, Paris, France

[3] CNRS, UMR 3525, Paris, France

Correspondence to :

Jacqueline Cherfils
Laboratoire de Biologie et Pharmacologie Appliquée,
CNRS and Ecole normale supérieure Paris-Saclay,
61 Avenue du Président Wilson
94235 Cachan CEDEX, France
jacqueline.cherfils@ens-paris-saclay.fr

bioRxiv preprint doi: https://doi.org/10.1101/323253; this version posted May 16, 2018. The copyright holder for this preprint (which was not certified by peer review) is the author/funder. All rights reserved. No reuse allowed without permission.

Abstract (250 words)

FIC proteins regulate molecular processes in bacteria and animals by carrying out various post-translational modifications (PTM) of proteins by phosphate-containing compounds. The most frequent FIC-catalyzed PTM is the addition of AMP using ATP as a cofactor, a reaction coined AMPylation. In a large subgroup of FIC proteins, AMPylation is inhibited by a structurally conserved glutamate, but a diffusible signal able to relieve autoinhibition has not been identified. Here, we addressed this issue by studying two members of this subgroup, a single-domain FIC protein from the bacterial pathogen *Enterococcus faecalis* (EfFIC) and human HYPE/FicD, which is involved in the unfolded protein response in the endoplasmic reticulum. By combining structural and biochemical analysis, we find that EfFIC catalyzes both AMPylation and deAMPylation, and that both enzymatic activities are borne by the same active site. Remarkably, the conserved glutamate implements a multi-position metal switch, whereby different metals support or inhibit each of these reactions. As a result, the balance between the AMPylation and deAMPylation activities of EfFIC is controlled by the Mg^{2+}/Ca^{2+} ratio, with Ca^{2+} favoring deAMPylation. Furthermore, we show that deAMPylation of the endoplasmic reticulum BIP chaperone by human FicD/HYPE is dependent on the Mg^{2+}/Ca^{2+} ratio, with high Ca^{2+} concentration impairing deAMPylation. Our findings suggest that the conserved glutamate is a signature of AMPylation/deAMPylation bifunctionnality in FIC proteins. They also identify for the first time a diffusible signal that can rapidly modulate these opposing activities, which opens important perspectives for their functions in bacterial stress and human ER homeostasis.

bioRxiv preprint doi: https://doi.org/10.1101/323253; this version posted May 16, 2018. The copyright holder for this preprint (which was not certified by peer review) is the author/funder. All rights reserved. No reuse allowed without permission.

Significance statement (120 words)

Many FIC proteins regulate target proteins by addition of AMP, a reaction coined AMPylation. In a large FIC proteins subgroup, AMPylation is autoinhibited by a conserved glutamate, but a diffusible activation signal has not been identified. Here we discover that the FIC protein from the pathogen *Enterococcus faecalis* catalyzes both AMPylation and deAMPylation and that its conserved glutamate implements a multi-position metal switch that controls the balance between these activities. Furthermore, we show that a metal, Ca^{2+}, also tunes deAMPylation of the BIP chaperone by the related human FicD/HYPE protein. These findings identify for the first time a diffusable signal that can rapidly tune FIC proteins, with important implications in bacterial stress and in the unfolded protein response in the ER.

bioRxiv preprint doi: https://doi.org/10.1101/323253; this version posted May 16, 2018. The copyright holder for this preprint (which was not certified by peer review) is the author/funder. All rights reserved. No reuse allowed without permission.

Introduction

In less than a decade, FIC proteins have emerged as a large family of enzymes controling the activity of target proteins by post-translationally modifying them with phosphate-containing compounds (reviewed in (1, 2 , 3 , 4)). These proteins are characterized by the presence of a conserved FIC domain, which carries out the post-translational modification (PTM) of a Tyr, Ser or Thr residue in a target protein (5 , 6 , 7 , 8 , 9 , 10 , 11). The most frequent PTM reaction catalyzed by FIC enzymes is the addition of AMP using ATP as a cofactor, coined AMPylation or adenylylation. This PTM activity was originally discovered in toxins from bacterial intracellular pathogens (12). It was later identified in bacterial toxin/antitoxins (e.g. (7)) and other bacterial FIC proteins of unknown functions (e.g. (11)), and in the only FIC protein found in metazoans, HYPE/FicD, which controls the reversible AMPylation of the BIP chaperone in the endoplasmic reticulum (ER) to match its activity to the load in unfolded proteins (13 , 14 , 15). A commonality of AMPylation and all other PTM reactions catalyzed by FIC proteins is that they use a motif of conserved sequence motif for catalysis, the FIC motif, which carries an invariant histidine that is critical for nucleophilic attack of the cofactor by the target residue, and an acidic residue (aspartate or glutamate) that binds an Mg^{2+} ion to stabilize the negative charges of the cofactor phosphates at the transition state (reviewed in (1, 2 , 3 , 4)).

Given their role in controling important bacterial and cellular responses, FIC-dependent PTM levels are expected to be precisely regulated. For instance, FIC toxin components of toxin-antitoxin modules are inhibited by obstruction of their active sites by their cognate antitoxin, and this strong inhibition is relieved by removal of the antitoxin (7 , 9 , 16). In a different strategy, addition of phosphocholine to cellular GTPases by *Legionella pneumophila* AnkX is reversed by another toxin, Lem3 (reviewed in (3)). Departing from these intermolecular mechanisms, an intriguing autoregulatory glutamate has been described in various AMPylating FIC proteins, which protrudes into the catalytic site from either N-terminal elements, as in human FicD (10), *Clostridum difficile* FIC (11) or *Shewanella oneidensis* FIC (17), or from a C-terminal α-helix as in single-domain FIC proteins from *Neisseria meningitidis* (7) and *Helicobacter pylori* (PDB 2F6S). This glutamate superimposes with an inhibitory glutamate from the VbhA antitoxin that blocks the ATP-binding site in its cognate VbhT toxin (7), and its mutation into Ala or Gly has been consistently shown to increase AMPylation activities *in vitro* and in cells (reviewed in (18)). Furthermore, crystal structures

bioRxiv preprint doi: https://doi.org/10.1101/323253; this version posted May 16, 2018. The copyright holder for this preprint (which was not certified by peer review) is the author/funder. All rights reserved. No reuse allowed without permission.

revealed that ATP binds to the active site of glutamate-containing FIC proteins in a manner where its γ-phosphate is not stabilized by interactions with the active site (7) and the α- and β-phosphates are bound in a non-canonical conformation (11), while mutation of the glutamate creates space such that the γ-phosphate can interact with the FIC active site (7). These observations led to propose that this conserved glutamate implements autoinhibition by impairing the utilization of ATP as a donor for AMP, hence that it must be displaced to allow productive binding of ATP (7). In *N. meningitidis* FIC (NmFIC), activation has been proposed to occur upon changes in toxin concentration (19). In this scheme, NmFIC is in an inactive tetrameric state at high concentration, which is further stabilized by ATP, while its dilution promotes its conversion to a monomeric state, leading to activation by displacement of the inhibitory glutamate followed by auto-AMPylations that reinforce its activation (19).

However, diffusible signals able to control autoinhibition in glutamate-bearing AMPylating FIC proteins have not been identified. In addition, in a recent new twist, metazoan HYPE/FicD was shown to carry out deAMPylation as its primary enzymatic activity, and the conserved glutamate was found to be critical for this reaction (20). These intringuing observations challenge the model in which autoinhibition by the conserved glutamate would be the sole mode of regulation of glutamate-containing AMPylating FIC proteins. In this study, we addressed this question by combining structural and biochemical analysis of a single-domain FIC protein from *Enterococcus faecalis* (EfFIC). Enteroccoci are commensals of the gastrointestinal tract that become pathogenic outside of the gut and cause difficult-to-treat infections in the hospital due to acquisition and transmission of antibiotic resistance (21 , 22). We discover that EfFIC has both AMPylation and deAMPylation activities borne by the same active site. Furthermore, the conserved glutamate implements a metal switch that allows the Mg^{2+}/Ca^{2+} ratio to tune the balance between these activities. Finally, we show that the metal switch also exists in human FicD/HYPE, whose deAMPylation of the ER chaperone BIP is decreased at high Ca^{2+}/Mg^{2+} ratio. These findings identify for the first time a diffusible signal that can rapidly and reversibly modulate the activity of glutamate-bearing AMPylating FIC proteins, with important implications for signaling in bacteria and animals.

bioRxiv preprint doi: https://doi.org/10.1101/323253; this version posted May 16, 2018. The copyright holder for this preprint (which was not certified by peer review) is the author/funder. All rights reserved. No reuse allowed without permission.

Results.

Structural basis for EfFIC AMPylation activity.

Enterococcus faecalis FIC belongs to class III FIC proteins, which are comprised of a single FIC domain and carry an autoinhibitory glutamate in their C-terminal α-helix. We determined crystal structures of unbound, phosphate-bound, AMP-bound and ATPγS-bound wild-type EfFIC ($EfFIC^{WT}$) and of unbound and sulfate-bound EfFIC carrying a mutation of the catalytic histidine into an alanine ($EfFIC^{H111A}$) (**Table 1 and Table S1**). These structures were obtained in different space groups, yielding 32 independent copies of the EfFIC monomer in various environments in the crystal. All EfFIC monomers resemble closely to each other and to structures of other class III FIC proteins (**Figure 1A**). Notably, the C-terminal α-helix that bears the inhibitory glutamate shows no tendency for structural flexibility, even in subunits that are free of intersubunit contacts in the crystal. The glutamate has the same conformation as in other glutamate-bearing FIC protein structures (**Figure 1B**) and is stabilized by intramolecular interactions and interactions with the nucleotide cofactor, when present (**Figure 1C**). Two crystal structures were obtained in co-crystallization with a non-hydrolyzable ATP analog (ATPγS), for which well-defined electron density was observed for the ADP moiety (**Figure S1A**). The positions of the α and β phosphates of ATPγS in these structures depart markedly from those seen in ATP bound unproductively to wild type NmFIC, in which only the ADP moiety is visible as in our structures (7), or bound non-canonically to CdFIC (11) (**Figure 1D**). In contrast, they superpose well to cofactors bound in a position competent for PTM transfer (7, 8) (**Figure 1E**). This observation prompted us to assess whether EfFIC is competent for AMPylation, using autoAMPylation which is a convenient proxy when the physiological target is not known (reviewed in (18)). Using [α-^{32}P]-ATP and autoradiography to measure the formation of AMPylated EfFIC (denoted $^{AMP*}EfFIC^{WT}$), we observe that $EfFIC^{WT}$ has conspicuous autoAMPylation activity in the presence of Mg^{2+} (**Figure 1F**). AMPylation is increased in $EfFIC^{E190G}$, in which the inhibitory glutamate is mutated into glycine, indicating that this activity is not optimal in $EfFIC^{WT}$ (**Figure 1F**). We conclude from these experiments that wild-type EfFIC has canonical features of an AMPylating FIC enzyme, and that the inhibitory glutamate mitigates this activity.

EfFIC is a deAMPylator in the presence of Ca^{2+}

bioRxiv preprint doi: https://doi.org/10.1101/323253; this version posted May 16, 2018. The copyright holder for this preprint (which was not certified by peer review) is the author/funder. All rights reserved. No reuse allowed without permission.

To gain further insight into the activity of EfFIC, we solved the crystal structure of EfFIC bound to AMP (EfFIC^{WT}-AMP) (**Table 1 and Table S1**). AMP superposes exactly to the AMP moiety of AMPylated CDC42 in complex with the FIC2 domain of the IbpA toxin (5) (**Figure 2A)**. Electron-rich density was observed next to AMP in the active site, corresponding to a calcium ion present in the crystallization solution to the exclusion of all other metal ions (**Figure S1B**). Ca^{2+} has 6 coordinations with distances in the expected 2.1-2.9 Å range, arranged with heptahedral geometry in which one ligand, which would be located opposite to one phosphate oxygen, is missing. It interacts with the phosphate of AMP, with the acidic residue in the FIC motif (Glu115), and with the inhibitory glutamate (Glu190) through a water molecule (**Figure 2B**). The position of Ca^{2+} in the EfFIC^{WT}-AMP structure differs from that of Mg^{2+} observed in other FIC protein structures in complex with ATP (**Figure 2C**), raising the intriguing issue that Ca^{2+} may play an alternative role in FIC functions. Inspired by the recent observation that animal HYPE/FicD proteins have deAMPylation enzymatic activity (20 , 23), we analyzed whether EfFIC would have deAMPylation activity in the presence of Ca^{2+}. Remarkably, the addition of Ca^{2+} induced conspicuous deAMPylation of EfFIC^{WT} that had been previously autoAMPylated in the presence of Mg^{2+} and [α-^{32}P]-ATP (**Figure 2D**).

In the above setup, the AMPylation and deAMPylation activities are acting concurrently. To characterize the deAMPylation reaction selectively, the hyperactive EfFIC^{E190G} mutant was autoAMPylated in the presence of Mg^{2+}, purified to remove ATP, PPi and Mg^{2+} such that no AMPylation remains possible, then its deAMPylation was triggered by addition of EfFIC^{WT} or an EfFIC mutant and of Ca^{2+}. The level of AMPylated EfFIC (denoted $^{AMP\text{-}FAM}$EfFIC) was quantified by fluorescence using ATP-FAM, an ATP analog fluorescently labeled on the adenine base. Robust deAMPylation was observed upon addition of EfFIC^{WT} and Ca^{2+} (**Figure 2E**, EfFIC^{WT} panel). No spontaneous deAMPylation of $^{AMP\text{-}FAM}$EfFIC^{E190G} was observed in the absence of EfFIC^{WT} (**Figure 2E**, control panel), indicating that the deAMPylation reaction occurs in trans. We used this deAMPylation setup to identify residues critical for de-AMPylation (**Figure 2E**, mutant panels). Mutation of the catalytic histidine (H111A) and of the metal-binding acidic residue in the FIC motif (E115A) impaired deAMPylation of $^{AMP\text{-}FAM}$EfFIC^{E190G}. EfFIC^{E190G}, which carries the mutation of the inhibitory glutamate, was also unable to promote deAMPylation, consistent with the absence of spontaneous deAMPylation in the assay. We conclude from these experiments that EfFIC is a

bioRxiv preprint doi: https://doi.org/10.1101/323253; this version posted May 16, 2018. The copyright holder for this preprint (which was not certified by peer review) is the author/funder. All rights reserved. No reuse allowed without permission.

bifunctional enzyme, that AMPylation and deAMPylation are borne by the same active site, and that the inhibitory glutamate is involved in the deAMPylation reaction.

The AMPylation and deAMPylation reactions are differentially regulated by metals.

The above results raises the issue of the nature of signals able to exploit the bifunctional active site of EfFIC to regulate AMPylation/deAMPylation alternation. Previous work showed that AMPylation of *Escherichia coli* DNA gyrase by NmFIC, which shares 56% sequence identity with EfFIC, was highly sensitive to the toxin concentration, with a sharp drop of activity above 250 μM (19). We used purified $^{AMP\text{-}FAM}EfFIC^{E190G}$ to analyze whether the deAMPylation activity of $EfFIC^{WT}$ would be similarly inhibited by increasing concentrations of $EfFIC^{WT}$ (1-2000 nM). As shown in **Figure 3A**, deAMPylation increased with $EfFIC^{WT}$ concentration, indicating that this reaction is not adversely affected by EfFIC concentration. Alternatively, the distinct electrochemical properties of $Ca^{2+}$and Mg^{2+} (reviewed in (24)) may allow them support AMPylation and deAMPylation differentially. Remarkably, Ca^{2+} was unable to support AMPylation, contrary to Mg^{2+} (**Figure 3B**). In contrast, both Mg^{2+} and Ca^{2+} supported potent deAMPylation (**Figure 3C, left panel**). Importantly, mutation of the inhibitory glutamate eliminated the ability of EfFIC to use Ca^{2+} for deAMPylation, while the mutant retained partial deAMPylation in the presence of Mg^{2+} (**Figure 3C, right panel**). To understand how Ca^{2+} affects AMPylation and deAMPylation differentially, we determined the crystal structure of $EfFIC^{WT}$-ATPγS-Ca^{2+}. Ca^{2+} is heptacoordinated to the α- and β-phosphates of ATPγS, of which only the ADP moiety is visible, to the inhibitory glutamate and to 4 water molecules (**Figure 3D**). In contrast, it does not form a direct or water-mediated interaction with the acidic residue in the FIC motif, which binds to Mg^{2+} in AMPylation competent structures {Engel, 2012 #33}. Remarkably, the position of Ca^{2+} is shifted with respect to that of Mg^{2+}, in a manner that Mg^{2+} and Ca^{2+} may compete with each other in AMPylation (**Figure 3E**). We tested this hypothesis by measuring the apparent AMPylation efficiency of $EfFIC^{WT}$ at different Mg^{2+}/Ca^{2+} ratio. As shown in **Figure 3F**, AMPylation is prominent when Mg^{2+} exceeds Ca^{2+}, while Ca^{2+} in excess over Mg^{2+} favors deAMPylation. We conclude from these experiments that AMPylation and deAMPylation efficiencies in EfFIC are regulated by a metal switch and that this regulatory mechanism is implemented by differential usage of the inhibitory glutamate and the acidic residue in the FIC motif for metal binding.

bioRxiv preprint doi: https://doi.org/10.1101/323253; this version posted May 16, 2018. The copyright holder for this preprint (which was not certified by peer review) is the author/funder. All rights reserved. No reuse allowed without permission.

DeAMPYlation of the BIP chaperone by human FicD/HYPE is tuned by Ca^{2+}

DeAMPylation has been recently identified as the primary activity of human HYPE/FicD (20), which features a glutamate structurally equivalent to the inhibitory glutamate in EfFIC (see **Figure 1B**, (10)) that is critical for deAMPylation of BIP (20). We analyzed whether, as observed in EfFIC, Mg^{2+} and Ca^{2+} metals could also affect FicD/HYPE activity, using fluorescent ATP-FAM to monitor BIP AMPylation levels. No measurable AMPylation of BIP by $HYPE^{WT}$ was observed, neither with Mg^{2+} nor Ca^{2+}, although $HYPE^{WT}$ itself showed some level of autoAMPylation with both metals (**Figure 4A**). Alternatively, we used $HYPE^{E234G}$, which carries the mutation of the conserved glutamate, to produce AMPylated BIP. Remarkably, while purified $^{AMP\text{-}FAM}$BIP was efficiently deAMPylated by $HYPE^{WT}$ in the presence of Mg^{2+}, no deAMPylation was measured in the presence of Ca^{2+} (**Figure 4B**). To determine whether FicD/HYPE does not bind Ca^{2+} or is unable to use it for deAMPylation, we carried out a Mg^{2+}/Ca^{2+} competition experiment in which $HYPE^{WT}$ and purified $^{AMP\text{-}FAM}$BIP were incubated at increasing Ca^{2+} concentration and a fixed Mg^{2+} concentration. As shown in **Figure 4C**, deAMPylation efficiency decreased as the Ca^{2+}/Mg^{2+} ratio increased, suggesting that Ca^{2+} inhibits deAMPylation by competing with Mg^{2+}. We conclude from these experiments that Ca^{2+} binds to FicD/HYPE in a catalytically incompetent manner, which allows it to tune the deAMPylation efficiency of FicD/HYPE towards the BIP chaperone.

Discussion

In this study, we sought after a diffusible signal able to regulate the large group of glutamate-bearing AMPylating FIC proteins. Combining structural and biochemical observations, we first show that bacterial EfFIC is a bifunctional enzyme that encodes AMPylating and deAMPylating activities and that both reactions use the same active site. Next, we discover that the balance between these opposing activities is controlled by a metal switch, in which each reaction is differentially supported and inhibited by Mg^{2+} and Ca^{2+} in a manner that the Mg^{2+}/Ca^{2+} ratio determines the net AMPylation level. Furthermore, we identify the inhibitory glutamate and the acidic residue in the FIC motif as residues essential for the metal switch. Finally, we show that deAMPylation of the endoplasmic reticulum BIP chaperone by human

bioRxiv preprint doi: https://doi.org/10.1101/323253; this version posted May 16, 2018. The copyright holder for this preprint (which was not certified by peer review) is the author/funder. All rights reserved. No reuse allowed without permission.

FicD/HYPE is also dependent on the Ca^{2+}/Mg^{2+} ratio, with high Ca^{2+} concentration impairing deAMPylation.

The identification of a potent deAMPylation activity in a bacterial FIC protein (this study) and in human FicD/HYPE (20), which depends on an equivalent glutamate in these otherwise remotely related FIC proteins, leads us to propose that the conserved glutamate is a signature of the ability of FIC proteins to catalyze both AMPylation and deAMPylation. Our data allow to delineate the catalytic basis for this bifunctionality, in which catalytic residues are shared by the AMPylation and deAMPylation reactions but have different roles in catalysis. In the AMPylation reaction, the invariant histidine in the FIC motif activates the acceptor hydroxyl of a target protein by attracting a proton and the acidic residue (Asp or Glu) in the FIC motif binds a metal that stabilizes the phosphates of the cofactor at the transition state (reviewed in (2 , 3)). Based on the observations that the α- and β-phosphates of ATP bind with canonical positions in wild-type EfFIC and that AMPylation is potentiated by mutation of the glutamate in various FIC proteins, we propose that the primary role of the glutamate in AMPylation is to mitigate the efficiency of this reaction in the presence of Mg^{2+}, possibly to match AMPylation and deAMPylation efficiencies. In the deAMPylation mechanism depicted in **Figure 5** (see also discussion in **Supplementary data and Figure S2**), the conserved glutamate activates a water molecule for nucleophilic attack of the phosphorus, and the invariant histidine generates the free hydroxyl group in the protein residue by giving up a proton, as also proposed in (20). In addition, both the acidic residue of the FIC motif and the conserved glutamate contribute to binding a catalytic metal, which stabilizes the phosphate of the AMP moiety at the transition state. A remarkable feature in the above bifunctional mechanism is that both reactions can be adversely regulated by a second metal that competes with the catalytic metal. In EfFIC, we observed that Ca^{2+} binds to ATP in a shifted position with respect to the canonical AMPylation Mg^{2+}-binding site, resulting in decreased AMPylation. In a similar scenario, Ca^{2+} competes with Mg^{2+} in the deAMPylation reaction catalyzed by FicD/HYPE, thereby decreasing deAMPylation. This multi-position metal switch constitutes a new paradigm in bifunctional enzyme regulation, in which the relative affinities of specific metals for the AMPylation and deAMPylation configurations tip the balance towards opposing activities within the same active site. Future studies are now needed to determine the bifunctionality spectrum of glutamate-bearing FIC proteins resulting from variations in metal specificities and affinities. Likewise, the observation by us and others that FicD/HYPE has distinct AMPylation and deAMPylation patterns towards itself and BIP suggests that the protein

bioRxiv preprint doi: https://doi.org/10.1101/323253; this version posted May 16, 2018. The copyright holder for this preprint (which was not certified by peer review) is the author/funder. All rights reserved. No reuse allowed without permission.

substrate influences the AMPylation/deAMPylation balance through mechanisms that are currently unknown. Finally, how other levels of regulation, such as autoAMPylation and changes in oligomerization that have been described for a close homolog of EfFIC (19), combine with the intrinsic metal switch identified in this study will have to be investigated.

Together, our findings identify for the first time a diffusible signal that can modulate the activity of glutamate-containing bacterial FIC proteins. This raises the issue of physiological conditions that can lead to a sharp variation of Ca^{2+} (or possibly another metal) levels in bacteria resulting in an AMPylation/deAMPylation switch. Bacterial FIC proteins are present in a large number of bacteria with unrelated lifestyles, where they must respond to specific stress situations. Although speculative at that stage, one such situation could thus be related to antimicrobial chemicals and peptides, which bacteria produce in vast variety for ecological competition purposes, some of which disrupt the integrity of the bacterial wall (reviewed in (25)). Because bacteria normally contain a low concentration of Ca^{2+}, increase of intracellular Ca^{2+} following leakage of the bacterial cell wall could be equated to a danger signal, calling for a defense response mediated by FIC proteins. How individual bacteria exploit the bifunctionality of their FIC proteins in their ecological niche or in infections will be an important issue to address in future studies.

Our observation that deAMPylation of the BIP chaperone by human HYPE is intrinsically sensitive to the Mg^{2+}/Ca^{2+} ratio, with Ca^{2+} restraining deAMPylation, suggests an appealing hypothesis for the regulation of FicD/HYPE in endoplasmic reticulum (ER) functions. Recently, FicD/HYPE has been demonstrated to stimulate the activity of the BIP chaperone in response to an increase in the unfolded protein load (13-15, 23), and this relies on its deAMPylation of BIP (20). Ca^{2+} is a fast and efficient messenger that is critical for ER homeostasis, where its depletion swiftly alters protein folding processes and activates the unfolded protein response (reviewed in (26 , 27)). It is thus tempting to speculate that inhibition of FicD/HYPE deAMPylation at high Ca^{2+}, which we observe *in vitro*, reflects its inhibition under ER homeostasis, where Ca^{2+} concentration is high and BIP activity is not required. Conversely, depletion of Ca^{2+} induces ER stress and triggers the UPR. Depletion of Ca^{2+} may thus release inhibition of FicD/HYPE, leading to efficient deAMPylation of BIP and up-regulation of its activity, which is a key feature of the UPR. In this model, FicD/HYPE functions as an integrator between Ca^{2+} homeostasis in the ER and the BIP-mediated unfolded protein response.

bioRxiv preprint doi: https://doi.org/10.1101/323253; this version posted May 16, 2018. The copyright holder for this preprint (which was not certified by peer review) is the author/funder. All rights reserved. No reuse allowed without permission.

In conclusion, we have identified a diffusable and rapidly tunable signal that can modulate the intrinsic enzymatic activity of glutamate-bearing FIC proteins and tip the balance between AMPylation and deAMPylation reactions, with major implications in bacterial and human physiology and a potential impact in infections and ER diseases. Future studies are now needed to investigate how the metal switch of glutamate-bearing FIC protein activities is exploited in bacterial stress, and, in the case of animal FiD/HYPE, its role in the unfolded protein response and its crosstalks with Ca^{2+}-controled processes in the ER.

bioRxiv preprint doi: https://doi.org/10.1101/323253; this version posted May 16, 2018. The copyright holder for this preprint (which was not certified by peer review) is the author/funder. All rights reserved. No reuse allowed without permission.

Figure Legends

Figure 1 : Structural basis for the AMPylation activty of EfFIC

A : Structure of the EfFIC monomer showing the FIC motif (pink), the C-terminal α-helix bearing the inhibitory glutamate (orange) and the β-hairpin predicted to bind protein substrates (cyan). The ADP moiety of ATPγS is shown in sticks.

B : The inhibitory glutamate from $EfFIC^{WT}$ (orange) is structurally equivalent to the glutamate found in the C-terminus of NmFIC ((7), PDB 2G03) and in the N-terminus of *Bacteroides* BtFIC (PDB 3CUC), *Clostridium* CdFIC ((11), PDB 4X2E) and of human FicD/HYPE ((10), PDB 4U04). Superpositions are done on the structurally highly conserved FIC motif.

C : Interactions of the inhibitory glutamate with the active site of ATPγS-bound $EfFIC^{WT}$. Hydrogen bonds are depicted by dotted lines.

D : The positions of the α- and β-phosphates of ATPγS bound to $EfFIC^{WT}$ (yellow) diverge from those of ATPγS bound to $NmFIC^{WT}$ (cyan, (7), PDB 3S6A) and of ATP bound to CdFIC (blue, (11), S31A/E35A mutant, PDB 4X2D) in a non-canonical conformations. Note that only the ADP moiety of ATPγS is visible in the $EfFIC^{WT}$ and $NmFIC^{WT}$ crystal structures.

E : The α- and β-phosphates of ATPγS bound to $EfFIC^{WT}$ (yellow) superpose well to those of ATP bound to NmFIC (purple, (7), E186G mutant, PDB 3ZLM) and of CDP-choline bound to AnkX (green, (8), H229A mutant, PDB 4BET) in a PTM-competent conformation.

F : AutoAMPylation of $EfFIC^{WT}$ and $EfFIC^{E190G}$. The level of AMPylated proteins (indicated as $^{AMP*}EfFIC^{WT}$) was measured by autoradiography using radioactive [α-^{32}P]-ATP in the presence of 100 nM Mg^{2+}. The reaction was carried out for one hour for $EfFIC^{WT}$ and five minutes for $EfFIC^{E190G}$. The total amount of $EfFIC^{WT}$ measured by Coomassie staining in the same sample is shown.

Figure 2 : EfFIC is a deAMPylator in the presence of Ca^{2+}

A : AMP bound to $EfFIC^{WT}$ superposes with the AMP moiety of AMPylated CDC42 in complex with the FIC protein IbpA ((5), PDB 4ITR). Superposition was carried out based on the FIC motif.

B : Close-up view of Ca^{2+} bound to $EfFIC^{WT}$-AMP. The incomplete heptagonal coordination sphere of Ca^{2+} is indicated by dotted lines. Water molecules are shown as red spheres.

bioRxiv preprint doi: https://doi.org/10.1101/323253; this version posted May 16, 2018. The copyright holder for this preprint (which was not certified by peer review) is the author/funder. All rights reserved. No reuse allowed without permission.

C: Ca^{2+} bound to $EfFIC^{WT}$-AMP is shifted with respect to Mg^{2+} bound to $NmFIC^{E/G}$-AMPPNP. The superposition is done on the FIC motif.

D : $EfFIC^{WT}$ has deAMPylation activity in the presence of Ca^{2+}. $EfFIC^{WT}$ was autoAMPylated in the presence 0.1 µM Mg^{2+} for one hour, then the sample was incubated for 60 minutes with EDTA alone (1mM) (lane 1) or 5, 30 and 60 minutes with EDTA (1mM) and an excess of Ca^{2+} (10 mM) (lanes 2-4). AMPylation levels were analyzed by autoradiography using [α-^{32}P]-ATP. The total amount of $EfFIC^{WT}$ measured by Coomassie staining in the same sample is shown.

E : Key residues of the AMPylation active site are required for deAMPylation. $EfFIC^{E190G}$ was auto-AMPylated for one hour in the presence of fluorescently-labeled ATP-FAM and Mg^{2+}, then $^{AMP\text{-}FAM}EfFIC^{E190G}$ was purified to remove Mg^{2+}, PPi and ATP-FAM. DeAMPylation was then triggered by addition of wild-type or mutant EfFIC as indicated in the presence or not of 1mM Ca^{2+}. AMPylation levels (indicated as $^{AMP\text{-}FAM}EfFIC^{E190G}$) after one hour incubation were analyzed by fluorescence. The total amount of EfFIC proteins (indicated as $EfFIC^{total}$) measured by Coomassie staining in the same sample is shown.

Figure 3 : The Mg^{2+}/Ca^{2+} ratio tunes the balance between EfFIC AMPylation and de-AMPylation

A : DeAMPylation is not inhibited at high EfFIC concentration. Purified $^{AMP\text{-}FAM}EfFIC^{E190G}$ was incubated with increasing concentrations of $EfFIC^{WT}$ for one hour in the presence of 100µM Ca^{2+}. AMPylation levels were measured by fluorescence as in **Figure 2D**.

B : $EfFIC^{WT}$ uses Mg^{2+} but not Ca^{2+} for autoAMPylation. AutoAMPylation was carried out at 1mM Ca^{2+} or Mg^{2+} for one hour and was measured by autoradiography as in **Figure 1F**.

C : The conserved glutamate of EfFIC is required for the usage of both Mg^{2+} and Ca^{2+} for deAMPylation. Experiments were carried out for one hour as in **Figure 3A** in the presence of 0.5mM EDTA and 3mM of Mg^{2+} or Ca^{2+}. Quantification of deAMPylation efficiencies is shown on the right panel.

D: Close-up view of Ca^{2+} bound to $EfFIC^{WT}$-ATPγS. The heptagonal coordination sphere of Ca^{2+} is indicated by dotted lines. Water molecules are shown as red spheres.

E : Ca^{2+} bound to $EfFIC^{WT}$-ATPγS is shifted with respect to Mg^{2+} bound to AMPylation-competent $NmFIC^{E/G}$-AMPPNP.

F: The net AMPylation efficiency of $EfFIC^{WT}$ is controled by the Mg^{2+}/Ca^{2+} ratio. Auto-AMPylation of $EfFIC^{WT}$ was carried out for one hour at fixed Mg^{2+} concentration (1mM) and

bioRxiv preprint doi: https://doi.org/10.1101/323253; this version posted May 16, 2018. The copyright holder for this preprint (which was not certified by peer review) is the author/funder. All rights reserved. No reuse allowed without permission.

Ca^{2+} concentrations ranging from 0 to 5.0 mM. $^{AMP\text{-}FAM}$EfFIC levels were measured by fluorescence. DeAMPylation levels are expressed as the percentage of the maximal AMPylation level obtained with Mg^{2+} alone. All measurements have p-values <0.05 with respect to the experiment containing Mg^{2+} alone. The total amount of $EfFIC^{WT}$ measured by Coomassie staining in each sample is shown.

Figure 4: DeAMPylation of BIP by FicD/HYPE requires Mg^{2+} and is inhibited by Ca^{2+}.

A: $HYPE^{WT}$ does not AMPylate the BIP chaperone. Reactions were carried for one hour in presence of 1mM Mg^{2+} or 1mM Ca^{2+}. The level of AMPylated proteins (indicated as $^{AMP\text{-}FAM}HYPE^{WT}$ and $^{AMP\text{-}FAM}$BIP) was measured by fluorescence. The total amount of proteins measured by Coomassie staining in the same sample is shown.

B: Ca^{2+} inhibits deAMPylation of BIP by $HYPE^{WT}$. BIP was first AMPylated for one hour by the hyperactive $HYPE^{E234G}$ mutant in the presence of 100 µM Mg^{2+}, then $^{AMP\text{-}FAM}$BIP was purified to remove Mg^{2+}, PPi and ATP-FAM. DeAMPylation of $^{AMP\text{-}FAM}$BIP was then triggered by addition of wild-type or mutant HYPE as indicated in the presence of 1mM Mg^{2+} or 1mM Ca^{2+}. $^{AMP\text{-}FAM}$BIP levels were measured by fluorescence. The total amount of BIP measured by Coomassie staining in each sample is shown.

C: The net deAMPylation efficiency of $HYPE^{WT}$ is tuned by the Mg^{2+}/Ca^{2+} ratio. DeAMPylation was carried out as in **Figure 4B** using a fixed Mg^{2+} concentration (200µM) and 0, 1, 2 or 3mM Ca^{2+}. AMPylation levels were measured by fluorescence, normalized to the fluorescence intensity of HYPE and expressed as the percentage of maximal deAMPylation level obtained in the absence of Ca^{2+}. All data have p-values <0.05 with respect to the control in the absence of Ca^{2+}. The total amount of BIP measured by Coomassie staining in each sample is shown.

Figure 5: Model of the Ca^{2+}-assisted deAMPylation catalytic mechanism.

In this model, the regulatory glutamate (Glu190 in EfFIC) attracts a proton from a water molecule coordinating the metallic cation (1) to activate it for nucleophilic attack of its oxygen on the phosphorus of AMP moiety in the AMPylated substrate (2). The positive charge provided by Ca^{2+} increases electrophilicity of the phosphorus and stabilizes the negative charge of the intermediate (2 and 3). The intermediate harboring a pentavalent phosphorus then rearranges, leading to the breaking of the phosphor-ester bond, which is elicited by the capture of a proton provided by the catalytic histidine (4). R : AMPylated protein

bioRxiv preprint doi: https://doi.org/10.1101/323253; this version posted May 16, 2018. The copyright holder for this preprint (which was not certified by peer review) is the author/funder. All rights reserved. No reuse allowed without permission.

Material and Methods.

Protein cloning, expression and purification

The codon-optimized gene encoding full-length *Enterococcus faecalis* EfFIC with an N-terminal 6-histidine tag was from GeneArt Gene Synthesis (ThermoFisher Scientific) and cloned into a pET22b(+) vector. The codon-optimized gene encoding human FicD/HYPE (residues 45-459) carrying an N-terminal 6-His tag followed by SUMO tag was from GeneArt Gene Synthesis and cloned into a pET151/D-TOPO vector (ThermoFisher Scientific). All mutations were performed with the QuickChange II mutagenesis kit (Agilent). *Mus musculus* BIP in pUJ4 plasmid is a kind gift from Ronald Melki (CNRS, Gif-sur-Yvette). All constructs were verified by sequencing (GATC). All EfFIC constructs were expressed in *E. coli* BL21 (DE3) pLysS in LB medium. Overexpression was induced overnight with 0.5 mM IPTG at 20°C. Bacterial cultures were centrifuged for 40 min at 4000g. Bacterial pellets were resuspended in lysis buffer (50 mM Tris-HCl pH 8.0, 150 mM NaCl, 5% glycerol, 0.25 mg/mL lysozyme) containing a protease inhibitor cocktail, disrupted at 125 psi using a high pressure cell disrupter and centrifuged 30 min at 22000g. The cleared lysate supernatant was loaded on a Ni-NTA affinity chromatography column (HisTrap FF, GE Healthcare) and eluted with 250 mM imidazole. Purification was polished by gel filtration on a Superdex 200 16/600 column (GE Healthcare) equilibrated with storage buffer (50 mM Tris-HCl pH 8.0, 150 mM NaCl). Wild-type and mutant FicD/HYPE were purified as EfFIC, except that the lysis buffer was complemented with 1mM DTT and 0.02% Triton X-100 and other buffers with 1mM DTT. To remove the SUMO tag, FicD/HYPE was incubated with SUMO protease (ThermoFischer) at 1/100 weight/weight ratio during 1 hour at room temperature. The cleaved fraction was separated by affinity chromatography (HisTrap FF, GE Healthcare) and further purified by gel filtration on a Superdex 200 10/300 column (GE Healthcare) equilibrated with storage buffer (50 mM Tris pH 8.0, 150 mM NaCl, 1mM DTT, 5% glycerol). Mouse BIP was purified as EfFIC.

Crystallization and structure determination

A summary of the crystal structures determined in this study is in **Table 1**. Proteins were crystallized using a TTP Labtech's Mosquito LCP crystallization robot and crystallization screens (Jena Bioscience and Quiagen). Conditions leading to crystals were subsequently

bioRxiv preprint doi: https://doi.org/10.1101/323253; this version posted May 16, 2018. The copyright holder for this preprint (which was not certified by peer review) is the author/funder. All rights reserved. No reuse allowed without permission.

optimized. Diffraction data sets were recorded at synchrotron SOLEIL and ESRF. Datasets were processed using XDS (28), xdsme (https://github.com/legrandp/xdsme) or autoProc (29). Structures were solved by molecular replacement and refined with the Phenix suite (30) or Buster (Bricogne G., Blanc E., Brandl M., Flensburg C., Keller P., Paciorek W.,Roversi P, Sharff A., Smart O.S., Vonrhein C., Womack T.O. (2017). BUSTER version 2.10.2. Cambridge, United Kingdom: Global Phasing Ltd.). Models were build using Coot (31). Softwares used in this project were curated by SBGrid (32). Crystallization conditions, data collection statistics and refinement statistics are given in **Table S1**. All structures have been deposited with the Protein Data Bank (PDB codes in **Table S1**).

AMPylation and deAMPylation assays

AMPylation and deAMPylation autoradiography assays were carried out using the following protocols. For AMPylation reactions, 8 µg of purified proteins were mixed with 10 µCi [α-32P] ATP (Perkin Elmer) in a buffer containing 50mM Tris-HCl pH 7.4, 150 mM NaCl and 0.1 mM $MgCl_2$. Reactions were incubated for 1 h at 30 °C, then stopped with reducing SDS sample buffer and boiling for 5 min. For deAMPylation, proteins were allowed to AMPylate as above for 1 h, then 1 mM EDTA was added with or without 10 mM $CaCl_2$. Proteins were resolved by SDS-PAGE and AMPylation was revealed by autoradiography.

EfFIC AMPylation and deAMPylation fluorescence assays were carried out using the following protocols. AMPylation was carried out using a fluorescent ATP analog modified by N^6-(6-Amino)hexyl on the adenine base (ATP-FAM, Jena Bioscience). AMPylated proteins were obtained by incubation for one hour at 30 °C in 50mM Tris pH 8.0, 150 mM NaCl, 0.1 mM $MgCl_2$ and an equimolar amount of ATP-FAM. Before deAMPylation reactions, the buffer was exchanged to 50 mM Tris-HCl pH 8.0 and 150 mM NaCl by 5 cycles of dilution/concentration on a Vivaspin-500 with a cut-off of 10kDa (Sartorius), resulting in a final dilution of ATP-FAM, $MgCl_2$ and PPi by about 10^5 times. DeAMPylation reactions were carried out using 2 µg of AMPylated protein and 4 µg of freshly purified EfFIC proteins in a buffer containing 50mM Tris-HCl pH 8.0 and 150 mM NaCl, for 1h at 30°C. Reactions were stopped by addition of reducing SDS sample buffer and boiling for 5 min. Proteins were resolved by SDS-PAGE and modification by AMP-FAM was revealed by fluorescence using green channel (excitation: 488 nm, emission: 526 nm) on a Chemidoc XR+ Imaging System (BioRad).

HYPE AMPylation and deAMPylation fluorescence assays were carried out using the

bioRxiv preprint doi: https://doi.org/10.1101/323253; this version posted May 16, 2018. The copyright holder for this preprint (which was not certified by peer review) is the author/funder. All rights reserved. No reuse allowed without permission.

following protocols. AMPylation was carried out using fluorescent ATP-FAM. AMPylated BIP was obtained by incubation for one hour at 30 °C in 50mM Tris pH 8.0, 150 mM NaCl, 0.1 mM $MgCl_2$, 2µM $HYPE^{E234G}$ and an equimolar amount of ATP-FAM. Before deAMPylation reactions, the buffer was exchanged with 50mM Tris-HCl pH 8.0 and 150 mM NaCl by 5 cycles of dilution/concentration on a Vivaspin-500 with a cut-off of 50kDa (Sartorius), resulting in a final dilution of ATP-FAM, $MgCl_2$ and PPi produced by the reaction of about 10^5 times. DeAMPylation reactions were carried using 2 µg of AMPylated protein and 4 µg of freshly purified $HYPE^{WT}$ in a buffer containing 50mM Tris pH 8.0 and 150 mM NaCl, for 1h at 30°C. Reactions were stopped and ATP-FAM modification revealed as EfFIC. Quantification of AMP-FAM levels was done using (ImageLab, BioRad).

All experiments were done at least in triplicate, except kinetics in Figure 3A that were done in duplicate.

Acknowledgements.

This work was supported by grants from the Fondation pour la Recherche Médicale and from the Agence Nationale pour la Recherche to J.C. and by grants n°ANR-10-LABX-62-IBEID and from the Fondation pour la Recherche Médicale to C.B. S.V. was supported by a PhD grant from the DIM MALINF and G.O. by a stipend from the Pasteur-Paris University International PhD program. We are grateful to the scientific teams at the PX1 and PX2 beamlines at the SOLEIL synchrotron (Gif-sur-Yvette, France) and from the ID29, ID30-A3 and ID30B beamlines at the European Synchrotron Research Facility (ESRF, Grenoble, France) for their expertise and advice. We thank Pascale Serror (INRA, Jouy-en-Josas, France) and Philippe Glaser (Institut Pasteur) for discussions and the members of the Cherfils lab for help and shared expertise.

bioRxiv preprint doi: https://doi.org/10.1101/323253; this version posted May 16, 2018. The copyright holder for this preprint (which was not certified by peer review) is the author/funder. All rights reserved. No reuse allowed without permission.

Table 1 – Summary of crystal structures of EfFIC determined in this study. All crystals have cell angles of α, β and γ = 90°. Crystallographic statistics are given in **Table S1**. * : only the ADP moiety is visible.

Form	Space group	Cell parameters *a*, *b*, *c* (Å)	Ligand	Resolution	PDB
WT	$P4_12_12$	65.13, 65.13, 248.06	PO_4^{2-}	2.29	6ER8
WT	I222	121.54, 131.00, 136.94	/	2.40	5NV5
WT	$P4_12_12$	64.98 64.98 246.24	AMP – Ca^{2+}	2.35	6EP0
WT	$P4_32_12$	125.35 125.35 362.8	ATPγS* – Ca^{2+}	2.15	6EP2
WT	$P4_32_12$	87.84 87.84 364.94	ATPγS*	1.93	6EP5
H118A	$P2_122_1$	76.67 77.11 103.15	/	2.60	5NWF
H118A	I222	121.93 131.16 136.71	SO_4^{2-}	2.20	5NVQ

bioRxiv preprint doi: https://doi.org/10.1101/323253; this version posted May 16, 2018. The copyright holder for this preprint (which was not certified by peer review) is the author/funder. All rights reserved. No reuse allowed without permission.

References

1. Kinch LN, Yarbrough ML, Orth K, & Grishin NV (2009) Fido, a novel AMPylation domain common to fic, doc, and AvrB. *PloS one* 4(6):e5818.
2. Garcia-Pino A, Zenkin N, & Loris R (2014) The many faces of Fic: structural and functional aspects of Fic enzymes. *Trends in biochemical sciences* 39(3):121-129.
3. Roy CR & Cherfils J (2015) Structure and function of Fic proteins. *Nat Rev Microbiol* 13(10):631-640.
4. Harms A, Stanger FV, & Dehio C (2016) Biological Diversity and Molecular Plasticity of FIC Domain Proteins. *Annu Rev Microbiol* 70:341-360.
5. Xiao J, Worby CA, Mattoo S, Sankaran B, & Dixon JE (2010) Structural basis of Fic-mediated adenylylation. *Nat Struct Mol Biol* 17(8):1004-1010.
6. Luong P, *et al.* (2010) Kinetic and structural insights into the mechanism of AMPylation by VopS Fic domain. *The Journal of biological chemistry* 285(26):20155-20163.
7. Engel P, *et al.* (2012) Adenylylation control by intra- or intermolecular active-site obstruction in Fic proteins. *Nature* 482(7383):107-110.
8. Campanacci V, Mukherjee S, Roy CR, & Cherfils J (2013) Structure of the Legionella effector AnkX reveals the mechanism of phosphocholine transfer by the FIC domain. *The EMBO journal* 32(10):1469-1477.
9. Castro-Roa D, *et al.* (2013) The Fic protein Doc uses an inverted substrate to phosphorylate and inactivate EF-Tu. *Nature chemical biology* 9(12):811-817.
10. Bunney TD, *et al.* (2014) Crystal structure of the human, FIC-domain containing protein HYPE and implications for its functions. *Structure* 22(12):1831-1843.
11. Dedic E, *et al.* (2016) A Novel Fic (Filamentation Induced by cAMP) Protein from Clostridium difficile Reveals an Inhibitory Motif-independent Adenylylation/AMPylation Mechanism. *The Journal of biological chemistry* 291(25):13286-13300.
12. Yarbrough ML, *et al.* (2009) AMPylation of Rho GTPases by Vibrio VopS disrupts effector binding and downstream signaling. *Science* 323(5911):269-272.
13. Sanyal A, *et al.* (2015) A novel link between Fic (filamentation induced by cAMP)-mediated adenylylation/AMPylation and the unfolded protein response. *The Journal of biological chemistry* 290(13):8482-8499.

bioRxiv preprint doi: https://doi.org/10.1101/323253; this version posted May 16, 2018. The copyright holder for this preprint (which was not certified by peer review) is the author/funder. All rights reserved. No reuse allowed without permission.

564 14. Ham H, *et al.* (2014) Unfolded protein response-regulated Drosophila Fic (dFic)
565 protein reversibly AMPylates BiP chaperone during endoplasmic reticulum
566 homeostasis. *The Journal of biological chemistry* 289(52):36059-36069.
567 15. Preissler S, *et al.* (2015) AMPylation matches BiP activity to client protein load in the
568 endoplasmic reticulum. *Elife* 4:e12621.
569 16. Stanger FV, Harms A, Dehio C, & Schirmer T (2016) Crystal Structure of the
570 Escherichia coli Fic Toxin-Like Protein in Complex with Its Cognate Antitoxin. *PloS*
571 *one* 11(9):e0163654.
572 17. Das D, *et al.* (2009) Crystal structure of the Fic (Filamentation induced by cAMP)
573 family protein SO4266 (gi|24375750) from Shewanella oneidensis MR-1 at 1.6 A
574 resolution. *Proteins* 75(1):264-271.
575 18. Veyron S, Peyroche G, & Cherfils J (2018) FIC proteins: from bacteria to humans and
576 back again. *Pathog Dis* 76(2).
577 19. Stanger FV, *et al.* (2016) Intrinsic regulation of FIC-domain AMP-transferases by
578 oligomerization and automodification. *Proceedings of the National Academy of*
579 *Sciences of the United States of America* 113(5):E529-537.
580 20. Preissler S, Rato C, Perera LA, Saudek V, & Ron D (2017) FICD acts bifunctionally
581 to AMPylate and de-AMPylate the endoplasmic reticulum chaperone BiP. *Nat Struct*
582 *Mol Biol* 24(1):23-29.
583 21. Hegstad K, Mikalsen T, Coque TM, Werner G, & Sundsfjord A (2010) Mobile genetic
584 elements and their contribution to the emergence of antimicrobial resistant
585 Enterococcus faecalis and Enterococcus faecium. *Clin Microbiol Infect* 16(6):541-554.
586 22. Lebreton F, *et al.* (2017) Tracing the Enterococci from Paleozoic Origins to the
587 Hospital. *Cell* 169(5):849-861 e813.
588 23. Casey AK, *et al.* (2017) Fic-mediated deAMPylation is not dependent on
589 homodimerization and rescues toxic AMPylation in flies. *The Journal of biological*
590 *chemistry* 292(51):21193-21204.
591 24. Carafoli E & Krebs J (2016) Why Calcium? How Calcium Became the Best
592 Communicator. *The Journal of biological chemistry* 291(40):20849-20857.
593 25. Hibbing ME, Fuqua C, Parsek MR, & Peterson SB (2010) Bacterial competition:
594 surviving and thriving in the microbial jungle. *Nat Rev Microbiol* 8(1):15-25.
595 26. Krebs J, Agellon LB, & Michalak M (2015) Ca(2+) homeostasis and endoplasmic
596 reticulum (ER) stress: An integrated view of calcium signaling. *Biochem Biophys Res*
597 *Commun* 460(1):114-121.

bioRxiv preprint doi: https://doi.org/10.1101/323253; this version posted May 16, 2018. The copyright holder for this preprint (which was not certified by peer review) is the author/funder. All rights reserved. No reuse allowed without permission.

598 27. Carreras-Sureda A, Pihan P, & Hetz C (2018) Calcium signaling at the endoplasmic
599 reticulum: fine-tuning stress responses. *Cell Calcium* 70:24-31.
600 28. Kabsch W (2010) Integration, scaling, space-group assignment and post-refinement.
601 *Acta crystallographica. Section D, Biological crystallography* 66(Pt 2):133-144.
602 29. Vonrhein C*, et al.* (2011) Data processing and analysis with the autoPROC toolbox.
603 *Acta crystallographica. Section D, Biological crystallography* 67(Pt 4):293-302.
604 30. Adams PD*, et al.* (2010) PHENIX: a comprehensive Python-based system for
605 macromolecular structure solution. *Acta crystallographica. Section D, Biological*
606 *crystallography* 66(Pt 2):213-221.
607 31. Emsley P & Cowtan K (2004) Coot: model-building tools for molecular graphics.
608 *Acta crystallographica. Section D, Biological crystallography* 60(Pt 12 Pt 1):2126-
609 2132.
610 32. Morin A*, et al.* (2013) Collaboration gets the most out of software. *Elife* 2:e01456.
611

bioRxiv preprint doi: https://doi.org/10.1101/323253; this version posted May 16, 2018. The copyright holder for this preprint (which was not certified by peer review) is the author/funder. All rights reserved. No reuse allowed without permission.

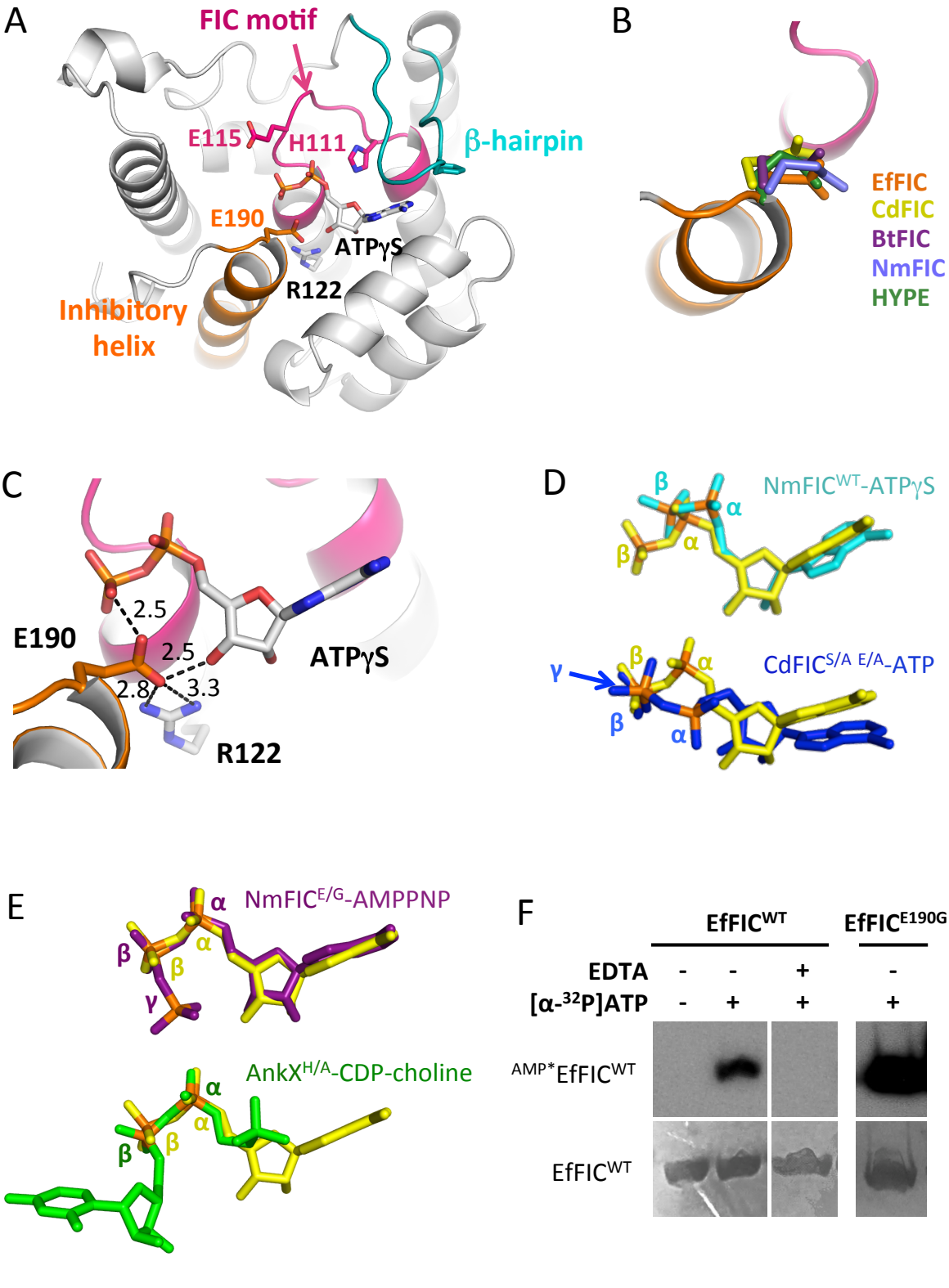

Figure 1

bioRxiv preprint doi: https://doi.org/10.1101/323253; this version posted May 16, 2018. The copyright holder for this preprint (which was not certified by peer review) is the author/funder. All rights reserved. No reuse allowed without permission.

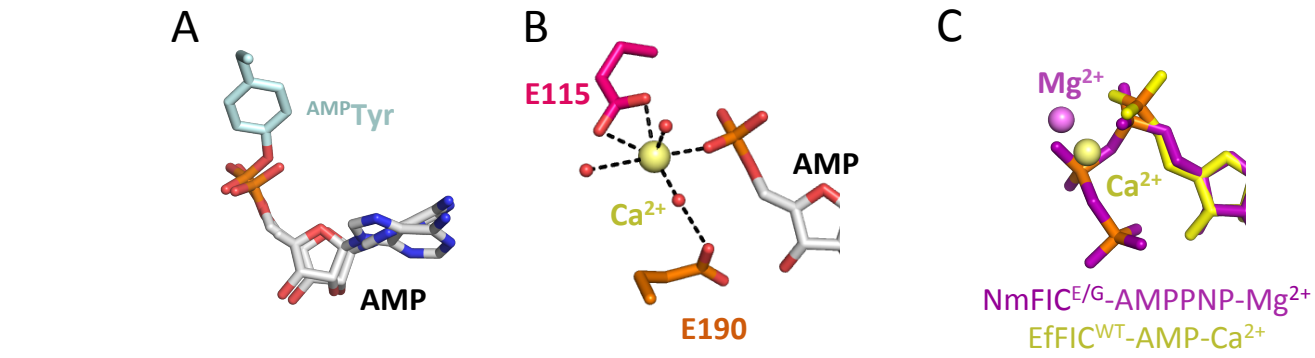

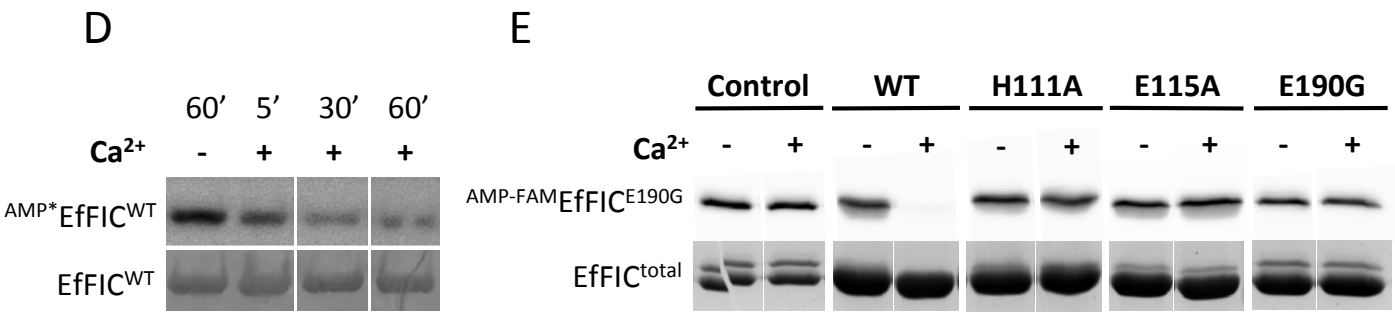

Figure 2

bioRxiv preprint doi: https://doi.org/10.1101/323253; this version posted May 16, 2018. The copyright holder for this preprint (which was not certified by peer review) is the author/funder. All rights reserved. No reuse allowed without permission.

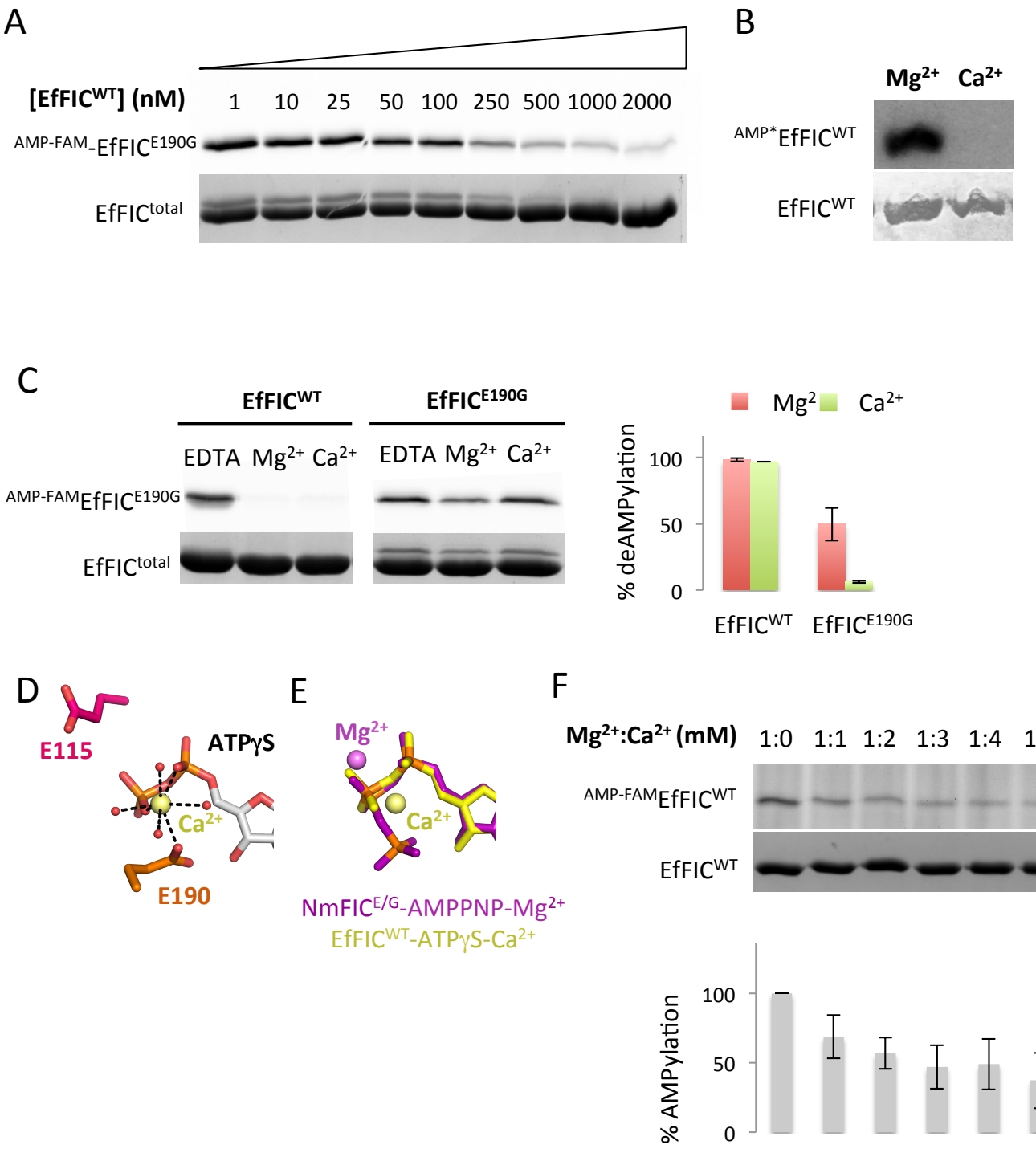

Figure 3

bioRxiv preprint doi: https://doi.org/10.1101/323253; this version posted May 16, 2018. The copyright holder for this preprint (which was not certified by peer review) is the author/funder. All rights reserved. No reuse allowed without permission.

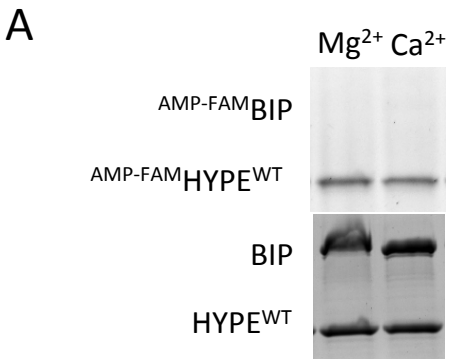

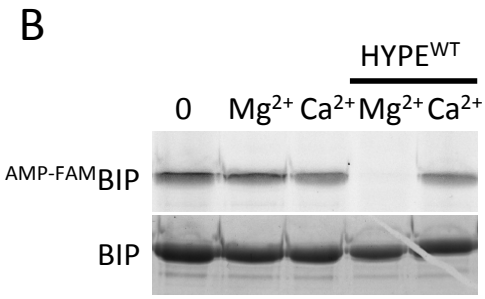

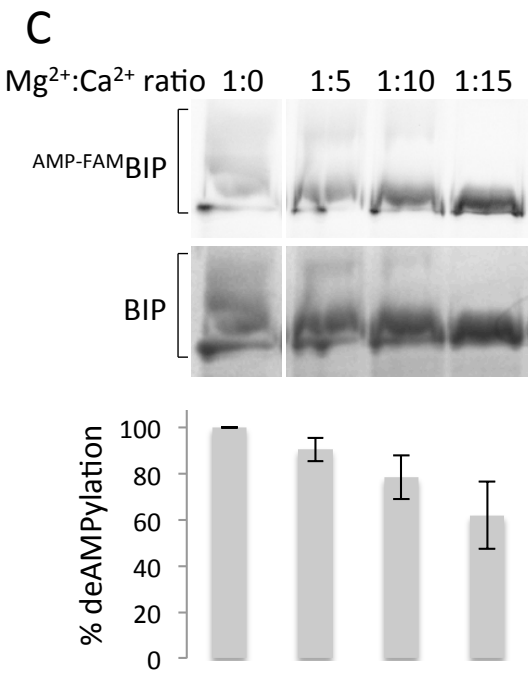

Figure 4

bioRxiv preprint doi: https://doi.org/10.1101/323253; this version posted May 16, 2018. The copyright holder for this preprint (which was not certified by peer review) is the author/funder. All rights reserved. No reuse allowed without permission.

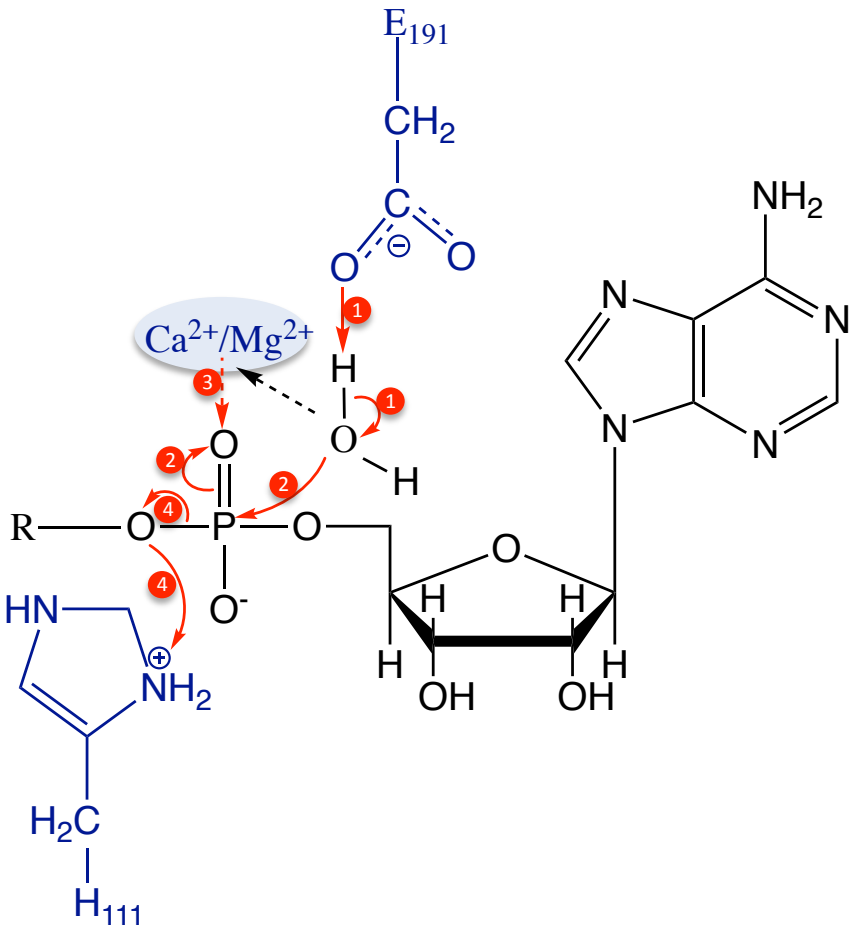

Figure 5